# A Grid Inductance Detection Method based on the Oscillation Characteristic of Inverter Terminal Voltage

Shuangming Duan, *Member, IEEE*, Bo Xia, Gangui Yan, *Member, IEEE*, Nan Li, Gen Li, *Member, IEEE*, and Yi Ding

***Abstract* - In grid-connected photovoltaic (PV) systems, grid inductance greatly influences the performance of grid-connected inverters. However, the grid inductance usually varies with the changes of the grid operation conditions. Therefore, accurate grid inductance detection is one of the key technologies to achieve an adaptive control of the grid-connected inverters under different operation conditions. In this paper, an equivalent circuit model of a grid-connected PV system which includes the controller, filter, and grid impedance is established. The oscillation characteristic of the inverter terminal voltage caused by the sudden change of the inverter output power is analyzed. The oscillation mechanism of the inverter terminal voltage caused by the interaction of the controller, filter, and grid impedance is investigated. A grid inductance detection method based on the oscillation characteristic of the inverter terminal voltage is proposed. The main advantage of the proposed method is that it does not need complicated signal processing and calculation procedures. A 10 kW grid-connected PV system was built for both simulations and the experimental setup. Finally, simulation and experimental results validate the correctness and effectiveness of the proposed method.**

***Index Terms* - Grid-connected PV systems, power sudden change, PV inverter, terminal voltage oscillation, grid inductance detection.**

## I. Introduction

With the increasing consumption of fossil fuels such as coal, oil, and natural gas, environmental problems have become increasingly serious. Distributed power generation technologies that utilize renewable energy to generate power has developed rapidly. The grid-connected inverters are the interfaces of the photovoltaic (PV) systems [1]-[3]. Considering that the grid-connected PV systems are distributed in the power grid, a large number of transformers and long transmission lines are required to access them to the grid, resulting in a very large grid impedance in the grid. Moreover, the change of the grid operation conditions may also lead to a big change of the grid impedance [4]. However, the grid inductance may greatly affect the control performance of grid-connected inverters as well as the stability of grid-connected PV systems [5]-[6]. To achieve an adaptive control of grid-connected inverters under different operation conditions, the grid inductance detection is of a great importance to provide a reference for the adjustment of the control parameters of grid-connected inverters [7]-[10].

At present, the methods for grid inductance detection are generally divided into passive (non-invasive) and active (invasive) [11]. Active methods deliberately create a disturbance in a grid and then the grid inductance can be estimated based on the grid responses. Active methods generally inject disturbance signals into the system, where the injected disturbance signals can be: 1) single frequency at 75 Hz [7], [12], [13], 600 Hz [14]; 2) dual frequencies at 400 Hz and 600 Hz [14]. Then, based on the current and voltage responses to this disturbance at PCC, the grid inductance can be estimated through Fourier analysis. To solve the shortcoming that these approaches only estimate the grid inductance at some specific frequencies, more spectrum information can be acquired by injecting pulse signals [15]. Roinila *et al*. [16] and Riccobono *et al*. [17] presented an approach by injecting pulse signals to estimate the grid inductance. Moreover, Neshvad *et al*. [18] proposed a method using pseudo-random-binary signals instead of pulse signals, which overcomes the shortcoming of the low detection accuracy when pulse signals are used to estimate grid inductance. For grid inductance detection of three-phase grid-connected inverters using *PQ* control, a disturbance is added to the references of active and reactive power, then grid inductance can be typically estimated by measuring voltage and current disturbances of two different operation points [19]-[23]. However, these methods are all carried out through injecting disturbance signals in a grid, and the grid inductance is detected based on the grid responses. Moreover, the disturbance signals may have an adverse effect on the output power quality and the stability of the grid-connected systems.

Different from active methods, passive methods use the non-characteristic harmonic voltage and current measurements inherently presented in the grid-connected systems to estimate the grid inductance [24]. Therefore, passive methods do not

Manuscript received March 10, 2021; revised May 19, 2021 and September 7, 2021; accepted December 23,2021. This work was supported in part by the Science and Technology Development Plan Program of Jilin, China under Grant 20200201198JC, in part by the Integrated project of National Natural Science Foundation of China under Grant No. U186660001. (*Corresponding author: Gangui Yan*).

Shuangming Duan, Bo Xia, Gangui Yan, Yi Ding are with Key Laboratory of Modern Power System Simulation and Control & Renewable Energy Technology, Ministry of Education (Northeast Electric Power University), Jilin 132012, China (e-mail: 33339371@163.com; xiab96820@163.com; yangg@neepu.edu.cn; dy354270443@163.com).

Nan Li is with state grid liaoning extra high voltage company, Shenyang 110000, China. (e-mail: 15526950008@163.com).

Gen Li is with the School of Electrical Engineering, Cardiff University, Cardiff, U.K.. (e-mail: LiG9@cardiff.ac.uk).

produce negative impact in the output power quality and the stability of grid-connected systems. Such methods have drawn extensive attention from researchers. But in most cases, this method may fail to provide accurate estimations [25]. Cobreces *et al*. [26] proposed a method based on a recursive least-squares algorithm to estimate the grid inductance. The structure and control algorithm of an inverter are not involved in modeling process, which may have a potential for wide applications. However, this method involves a huge burden of calculations and the shortcoming of low accuracy. One approach estimates the grid inductance via the excitation and detection of *LCL* filter resonances [27]. However, such a method may be unsecure due to the resonance amplification. In [28], the extended Kalman Filter proves to be beneficial to estimate the grid inductance. Moreover, this method can be a promising tool for estimating the grid inductance. However, the extended Kalman Filter is complicated due to the large system state-space models and Jacobian Matrix calculation. The tuning of noise covariance matrices (including the measurement and process covariance matrices) is difficult as well, especially when there is a huge number of states. In practice, the tuning is often a trial-and-error procedure [29]. Therefore, this method requires a system model simplification, which may reduce the accuracy of the model. In [30], an impedance identification scheme for three-phase balanced voltage source inverter based on the transient response of the inverter. However, the scheme is only designed to present an identification procedure of the impedance of the inverter with capacitive output. In [31], an inductance identification method based on the evaluation of the closed-loop transient of *dq*-axis is proposed. However, this method needs complicated iterative processes.

In this paper, a passive online detection method of grid inductance based on the transient response of inverter terminal voltage is proposed. This method does not need complicated signal processing and calculation procedures. The rest of this paper is organized as follows. An equivalent circuit model of a grid-connected PV system is established, and the mechanism of the interaction of the controller, filter, and grid impedance is investigated in Section II. In Section III, the oscillation characteristic of the inverter terminal voltage caused by the sudden changes of the inverter output power is analyzed, and a grid inductance detection method based on the oscillation characteristic of the inverter terminal voltage is proposed. In Sections IV and V, the correctness and effectiveness of the proposed method are verified by simulations in PSCAD/EMTDC and validated through experiments. Section VI makes conclusion and closes the paper.

## II. Analytical Model of The Grid-connected Inverter Terminal Voltage

Fig. 1 describes an *LC*-type grid-connected PV system. $L_1$ and $C_1$ are the filter inductance and the filter capacitance, respectively. $L_2$ is the common mode inductance. As a common practice, we model the grid as a series connection of resistance $R_g$, inductance $L_g$, and voltage sources $e_x$ [22], [28]. $u_{dc}$ is the DC bus voltage. $u_{sx}$ and $i_x$ are output voltage and output current of the inverter, respectively. $i_{gx}$ is the grid side current. $u_x$ is the filter capacitance voltage of the inverter ($x$=a, b, c), which is called inverter terminal voltage in this paper. PCC denotes the coupling point between the inverter and the grid.

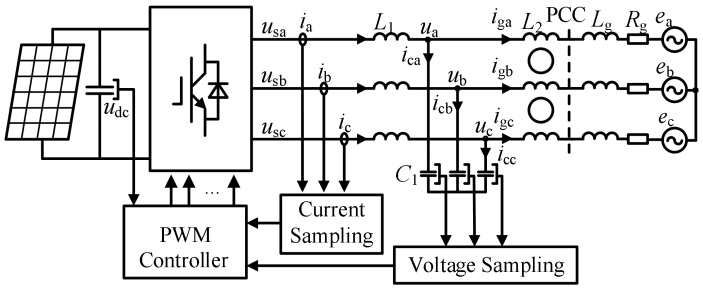

Fig. 1. Schematic diagram of a grid-connected PV system.

In the synchronous rotation reference frame (Park transformation), the circuit equations of the grid-connected PV system in Fig. 1 are given in the following equations. Generally, *d*-axis of the synchronous rotation reference frame coincides with the terminal voltage vector. The *q*-axis lags the *d*-axis by 90°. $i_d$ is the current component of *d*-axis, and defined as the active current. $i_q$ is the current component of *q*-axis, and defined as the reactive current.

$$\begin{cases} i_d = -\omega_1 C_1 u_q + C_1 \dfrac{du_d}{dt} + i_{dg} \\ i_q = \omega_1 C_1 U_d + C_1 \dfrac{du_q}{dt} + i_{qg} \end{cases} \tag{1}$$

$$\begin{cases} u_{sd} = -\omega_1 L_1 i_q + L_1 \dfrac{di_d}{dt} + u_d \\ u_{sq} = \omega_1 L_1 i_d + L_1 \dfrac{di_q}{dt} + u_q \end{cases} \tag{2}$$

$$\begin{cases} u_d = -\omega_1 L_{2g} i_{qg} + L_{2g} \dfrac{di_{dg}}{dt} + R_g i_{dg} + e_d \\ u_q = \omega_1 L_{2g} i_{dg} + L_{2g} \dfrac{di_{qg}}{dt} + R_q i_{qg} + e_q \\ L_{2g} = L_2 + L_g \end{cases} \tag{3}$$

where $u_{sd}$ and $u_{sq}$ are the *dq*-axis components of $u_{sx}$. $u_d$ and $u_q$ are the *dq*-axis components of $u_x$. $e_d$ and $e_q$ are the *dq*-axis components of $e_x$. $i_d$ and $i_q$ are the *dq*-axis components of $i_x$. $i_{dg}$ and $i_{qg}$ are the *dq*-axis components of $i_{gx}$ ($x$=a, b, c). $\omega_1$ is the grid voltage angular frequency.

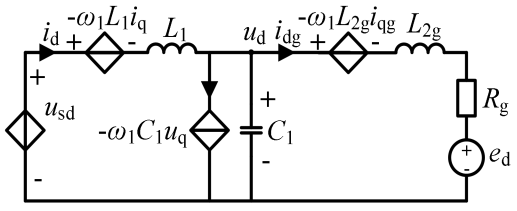

(a)

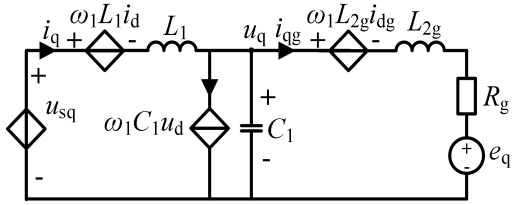


(b)

Fig. 2. Equivalent circuit model of the grid-connected system in *dq*-frame. (a) *d*-axis equivalent circuit model; (b) *q*-axis equivalent circuit model.

Fig. 2 shows the equivalent circuit model of the grid-connected system in *dq*-frame based on (1)-(3). The control strategy of the controlled voltage sources $u_{sd}$ and $u_{sq}$ in Fig. 2 is shown in (4). Fig. 3 shows the control system of the grid-connected inverter.

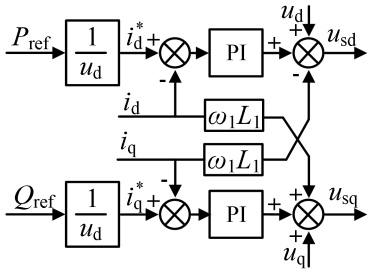


Fig. 3. Output voltage control schematic of the grid-connected inverter.

$$\begin{cases} u_{sd} = K_p\left(i_d^* - i_d\right) + K_i\int\left(i_d^* - i_d\right)dt - \omega_1 L_1 i_q + u_d \\ u_{sq} = K_p\left(i_q^* - i_q\right) + K_i\int\left(i_q^* - i_q\right)dt + \omega_1 L_1 i_d + u_q \end{cases} \tag{4}$$

The grid-connected inverter adopts a single synchronous reference frame phase-locked loop (SSRF-SPLL) system based on the symmetrical component method [32]. The system decomposes the grid voltage into positive and negative sequences, and uses the positive sequence component as the input signal of the phase-locked loop. The input signal of the phase-locked loop is not affected by the oscillation, and the obtained phase-locked loop angle remains unchanged. Therefore, there the dynamic characteristic of the phase-locked loop is not considered in this study. Moreover, ignoring the delays of sampling devices and switching devices, substitution of (4) into (2) gives

$$\begin{cases} K_p\left(i_d^* - i_d\right) + K_i\int\left(i_d^* - i_d\right)dt - \omega_1 L_1 i_q + u_d \\ = -\omega_1 L_1 i_q + L_1\dfrac{di_d}{dt} + u_d \\ K_p\left(i_q^* - i_q\right) + K_i\int\left(i_q^* - i_q\right)dt + \omega_1 L_1 i_d + u_q \\ = \omega_1 L_1 i_d + L_1\dfrac{di_q}{dt} + u_q \end{cases} \tag{5}$$

From (5), the control block of $i_d$ is presented in Fig. 4, and the control block of $i_q$ is the same as $i_d$.

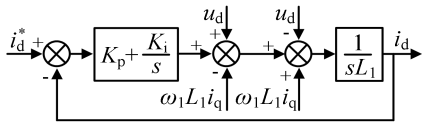


Fig. 4. Control block of $i_d$.

According to Fig. 4, the transfer function of the current control loop is derived as

$$W_{ci}(s) = \frac{i_d(s)}{i_d^*(s)} = \frac{i_q(s)}{i_q^*(s)} = \frac{sK_p + K_i}{s^2 L_1 + K_p s + K_i} \tag{6}$$

Furthermore, it is derived from (6) that

$$i_d(s) = \frac{sK_p + K_i}{s^2 L_1 + K_p s + K_i} i_d^*(s) \tag{7}$$

Then, the grid-connected inverter can be equivalent to a controlled current source. The output current of the grid-connected inverter is $i_d$, whose control coefficient is $W_{ci}(s)$. When the reference power generation $P_{ref}$ of the grid-connected PV system steps, it will lead to a sudden jump of the reference current $i_d^*$, as shown in Fig. 3. From (7), reference current $i_d^*$ will then affect the controlled current source $i_d$, which will result in interactions of the controller, filter, grid impedance and grid. Fig. 5 presents the equivalent circuit models of the grid-connected system in *dq*-frame.

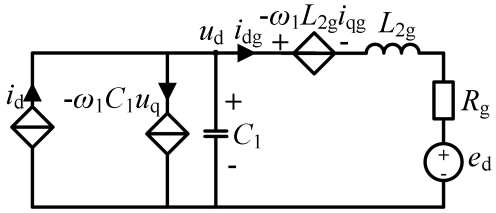


(a)

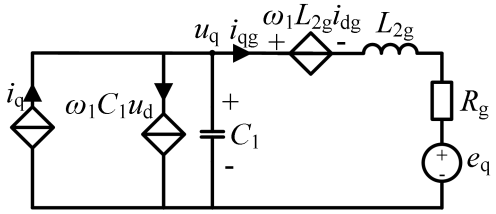


(b)

Fig. 5. Equivalent model of overvoltage analysis of the grid-connected system in *dq*-frame. (a) *d*-axis equivalent circuit model; (b) *q*-axis equivalent circuit model.

In this paper, the grid-connected inverters are considered using the vector positioning control of the inverter terminal voltage, and operate in the unit power factor mode. $i_q$ and $u_q$ are both equal to zero. In the transient process of sudden changes of the inverter output power, the inverter still works in the unit power factor mode, $i_q$ and $u_q$ are still equal to zero. Therefore, the effect of the *q*-axis equivalent circuit model can be ignored in the analysis. The *d*-axis equivalent circuit model can be directly used to characterize the transient process of the grid-connected system caused by the sudden changes of the inverter output power.

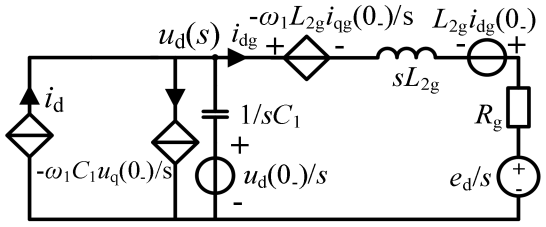


Fig. 6. Operational circuit of equivalent model for the grid-connected system terminal voltage analysis.

## III. A Theory of Grid Inductance Detection

Fig. 6 shows the operational circuit of the equivalent model in Fig. 5 (a). Fig. 6 illustrates that the inverter terminal voltage response caused by the sudden changes of the inverter output power is composed of the response of grid voltage $e_d$, the zero state response caused by the controlled current source $i_d$, and zero input responses caused by the initial value of the state quantity $u_q(0_-)$, $u_d(0_-)$, $i_{qg}(0_-)$, and $i_{dg}(0_-)$. Considering that grid-connected inverter normally operates in the unit power factor mode, $u_q(0_-)$ and $i_{qg}(0_-)$ are both equal to zero. Therefore, only $e_d$, $i_d$, $u_d(0_-)$, and $i_{dg}(0_-)$ work in the operational circuit of the equivalent model in Fig. 6. The time-domain expression of the controlled current source $i_d$ in Fig.6 can be expressed by (8)

$$i_d(t) = i_d^* + A_1 e^{\alpha_1 t} + A_2 e^{\alpha_2 t} \tag{8}$$

When $i_d$, $u_d(0_-)$, $e_d$ and $i_{dg}(0_-)$ act respectively, the responses of the inverter terminal voltage $u_{d1}(t)$, $u_{d2}(t)$, $u_{d3}(t)$, and $u_{d4}(t)$ are derived as

$$\begin{aligned} u_{d1}(t) = {} & B_1 e^{\beta t}\cos(\omega t) + B_2 e^{\beta t}\sin(\omega t) + \\ & B_3 e^{\alpha_1 t} + B_4 e^{\alpha_2 t} + i_d^* R_g \end{aligned} \tag{9}$$

$$\begin{aligned} u_{d2}(t) = {} & u_d(0_-) e^{\beta t}\cos(\omega t) + \\ & \frac{R_g u_d(0_-)}{2L_{2g}\sqrt{\frac{1}{L_{2g}C_1} - \frac{R_g^2}{4L_{2g}^2}}} e^{\beta t}\sin(\omega t) \end{aligned} \tag{10}$$

$$\begin{aligned} u_{d3}(t) = {} & e_d - e_d e^{\beta t}\cos(\omega t) - \\ & \frac{R_g e_d}{2L_{2g}\sqrt{\frac{1}{L_{2g}C_1} - \frac{R_g^2}{4L_{2g}^2}}} e^{\beta t}\sin(\omega t) \end{aligned} \tag{11}$$

$$u_{d4}(t) = -\frac{i_{dg}(0_-)}{C_1\sqrt{\frac{1}{L_{2g}C_1} - \frac{R_g^2}{4L_{2g}^2}}} e^{\beta t}\sin(\omega t) \tag{12}$$

Based on the superposition rule, the full response of the inverter terminal voltage can be further derived as

$$\begin{aligned} u_d(t) = {} & u_{d1}(t) + u_{d2}(t) + u_{d3}(t) + u_{d4}(t) = \\ & D_1 e^{\beta t}\cos(\omega t) + D_2 e^{\beta t}\sin(\omega t) + \\ & D_3 e^{\alpha_1 t} + D_4 e^{\alpha_2 t} + e_d + i_d^* R_g \end{aligned} \tag{13}$$

where $\alpha_1$, $\alpha_2$, and $\beta$ are the attenuation coefficients of the transient components, and $\omega$ is the oscillation angular frequency of the inverter terminal voltage. The expressions are as follows:

$$\alpha_1 = \frac{-\frac{K_p}{L_1} + \sqrt{\frac{K_p^2}{L_1^2} - \frac{4K_i}{L_1}}}{2} \tag{14}$$

$$\alpha_2 = \frac{-\frac{K_p}{L_1} - \sqrt{\frac{K_p^2}{L_1^2} - \frac{4K_i}{L_1}}}{2} \tag{15}$$

$$\beta = -\frac{R_g}{2L_{2g}} \tag{16}$$

$$\omega = \sqrt{\frac{1}{L_{2g}C_1} - \left(\frac{R_g}{2L_{2g}}\right)^2} \tag{17}$$

From (13), the inverter terminal voltage amplitude is determined by the controller parameters, filter parameters, grid impedance, the initial value of the state quantity, and the change value of the state quantity. From (14)-(16), the inverter terminal voltage attenuation time is determined by the controller parameters, filter inductance $L_1$, grid inductance $L_g$, and grid resistance $R_g$. From (17), the inverter terminal voltage oscillation frequency is determined by the filter capacitance $C_1$, grid inductance $L_g$, and grid resistance $R_g$.

According to the characteristic of the inverter terminal voltage oscillation frequency which is related to grid impedance during sudden change of the inverter output power, the grid inductance parameters can be obtained. In practical grid-connected PV systems, the grid inductance and filter inductance are in mH. The grid resistance is in mΩ. The filter capacitance is in μF. In (17), $(R_g/2/L_{2g})^2$ is far less than $(1/L_{2g}/C_1)$, which can be ignored. Therefore, we can simplify the frequency expression (17) as follow:

$$L_g = \frac{1}{\omega^2 C_f} - L_2 \tag{18}$$

This method uses the inherent oscillation characteristic of the inverter terminal voltage during sudden changes of the output power of a grid-connected system. The grid inductance can be obtained through the oscillation frequency. This method does not need to add additional signal generating devices and create new excitation signals. It also does not need complicated signal processing and calculation procedures. It should be mentioned that the proposed method and theoretical analysis are based on such terminal voltage oscillation phenomenon caused by the "sudden change" which is a fast and large power step-change artificially created in testing only. If the power change is not a "sudden change", there would be no such obvious oscillation of the terminal voltage. Therefore, the proposed method would not affect normal operation, power quality and other equipment at the PCC.

## IV. Simulation Verification

The 10 kW grid-connected PV system in Fig. 1 is built in PSCAD/EMTDC with the system parameters shown in Table I. The simulation analyzed the electromagnetic transient process of a grid-connected PV system under sudden changes of the output power of the grid-connected inverter. The effectiveness that the oscillation mechanism of the inverter terminal voltage caused by the sudden changes of the grid-connected inverter output power, and the theory of the grid inductance detection proposed in this paper are both verified. In the simulation, in order to obtain the responses of sudden changes of the grid-connected inverter output power, the grid-connected inverter is set to work in the non-MPPT state, and the grid-connected inverter reference generation power $P_{ref}$ is changed through the controller. After obtaining the inductance, the grid-connected inverter would be reset to the MPPT state.

TABLE I
PARAMETERS FOR THE PV SIMULATION SYSTEM

| Parameters | Symbols | Values |
|---|---|---|
| Filter capacitance | $C_1$ | 3.3 μF |
| Filter inductance | $L_1$ | 5.0 mH |
| Common mode inductance | $L_2$ | 0.1 mH |
| Grid inductance | $L_g$ | 0.9 mH |
| Grid resistance | $R_g$ | 200 mΩ |
| Voltage angular frequency | $\omega_1$ | 314 rad/s |
| Grid voltage | $e_x$ | 220 V |
| Proportion coefficient | $K_p$ | 200 |
| Integral coefficient | $K_i$ | 10000 |
| PWM frequency | $f_{PWM}$ | 20 kHz |

The power sudden change is intentionally set at the peak of $u_a$ ($t_0$=1.005 s), It is because that when the terminal voltage is at the peak moment, the initial value of the terminal voltage will be comparatively large, and therefore, the terminal voltage oscillation amplitude will be easier to be observed and recorded. Fig.7 presents the simulation waveforms of the inverter terminal voltage, the grid voltage, and the inverter output current when the grid-connected inverter reference generation power $P_{ref}$ was changed from 1.5 kW to 3.0 kW.

Fig. 7(b) illustrates that grid-connected inverter output power steps, and $i_d$ rises instantaneously, which further causes the inverter terminal voltage oscillation. Sudden changes of the inverter output power and the grid inductance are conducted to further verify the effectiveness of the proposed analysis of the inverter terminal voltage oscillations.

Fig. 8(a) illustrates that the inverter terminal voltage oscillation amplitude changes under different sudden changes of the grid-connected inverter output power. However, it should be noted that oscillation frequency of the inverter terminal voltage remains unchanged. Fig. 8(b) shows that the oscillation amplitude and frequency of the inverter terminal voltage both change when grid inductance changes. It can be concluded that the frequency of the inverter terminal voltage is only related to the grid inductance, and is not related to the sudden changes of the grid-connected inverter output power, which is consistent with the above theoretical analysis.

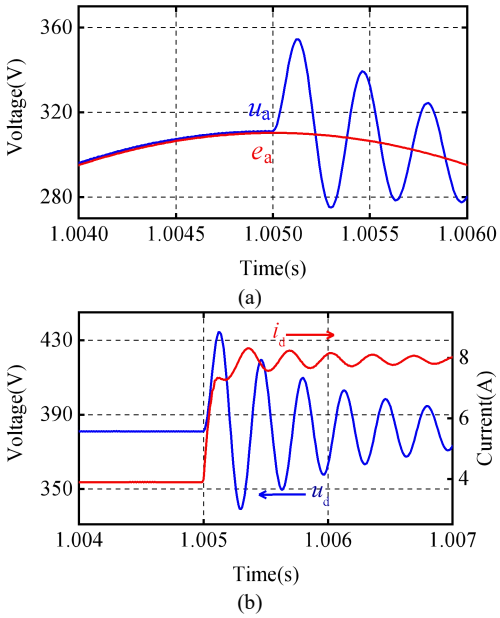


Fig. 7. Simulation waveforms of the grid-connected inverter when the sudden change of the grid-connected inverter output power. (a) Inverter terminal voltage ($u_a$) and grid voltage ($e_a$); (b) Inverter terminal voltage ($u_d$) and inverter output current ($i_d$).

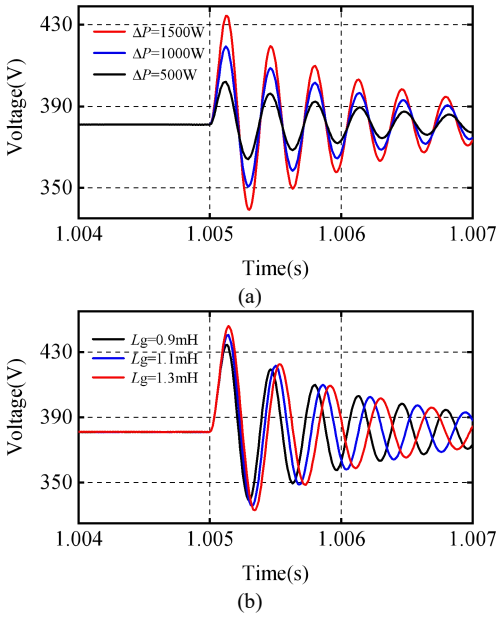


Fig. 8. Responses of the sudden inverter terminal voltage ($u_d$ in $dq$-frame) when system parameters changes. (a) Under different sudden changes of the grid-connected inverter output power; (b) the change of the grid inductance.

The effectiveness of the theory of grid inductance detection based on oscillation characteristic of the inverter terminal voltage is further verified. From the system parameters in Table I, the currents and voltages [in (8) and (13)] before and after the output power sudden change are changed into

$$i_d(t) = 8.00 - 3.95e^{-39550(t-t_0)} + 0.0049e^{-50.06(t-t_0)} \quad (19)$$

$$u_d(t) = 380.00 - 25.17e^{-100.00(t-t_0)}\cos(17407.48t) + 51.38e^{-100.00(t-t_0)}\sin(17407.48t) + 25.17e^{-39550.00(t-t_0)} + 0.00074e^{-50.06(t-t_0)} \quad (20)$$

Fig. 9 shows the waveforms of (19) and (20). From the simulation results in Fig. 7(a), the measured inverter terminal voltage oscillation frequency is 2849.34 Hz. From (17), the theoretical calculation inverter terminal voltage oscillation frequency in Fig. 9 is 2771.89 Hz, which is 77.45 Hz different from the simulation result, and the theoretical calculation error is 2.79%. The grid inductance $L_g$ calculation result is 0.846 mH through the oscillation frequency, and the detection accuracy is 94.0%. In this paper, the oscillation frequency characteristic of the inverter terminal voltage is investigated, and the oscillation attenuation characteristic of the inverter terminal voltage is not accurately considered. But the attenuation characteristic of the inverter terminal voltage does not affect measurement results of the inverter terminal voltage oscillation frequency. Therefore, the attenuation time in Fig. 9 can be ignored.

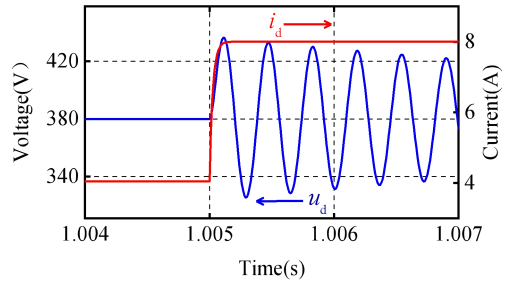


Fig. 9. Calculation waveforms of $i_d$ and $u_d$.

The sudden changes of the grid-connected inverter output power and the grid inductance are conducted to further verify the effectiveness of the proposed method of grid inductance detection. In the simulation, the grid inductance $L_g$ is 0.9 mH. Fig. 10 presents the simulation waveforms of the inverter terminal voltage and grid voltage under different sudden changes of the grid-connected inverter output power. The grid inductance detection values and detection accuracy are shown in Table II.

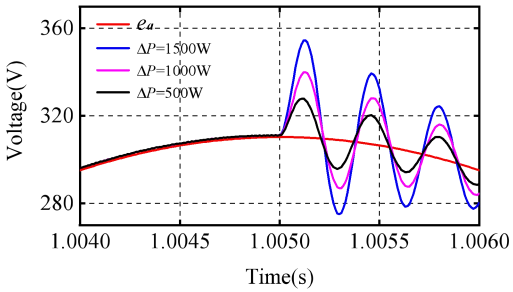


Fig. 10. Simulation waveforms of the inverter terminal voltage ($u_a$) and grid voltage ($e_a$) under different sudden changes of the grid-connected inverter output power.

From the simulation results in Fig. 10, the oscillation amplitudes of the inverter terminal voltage changes under different sudden changes of the grid-connected inverter output power. However, the oscillation frequency of the inverter terminal voltage remains unchanged. Detection results in Table II show that the grid inductance detection accuracy maintains within the range of 90% - 95%.

TABLE II
SIMULATION RESULTS OF DIFFERENT POWER VARIATIONS

| Power Variations (W) | Inductance (mH) | Accuracy (%) |
|---|---|---|
| 500 | 0.846 | 94.0 |
| 1000 | 0.839 | 93.2 |
| 1500 | 0.842 | 93.5 |

In the simulation, the sudden change of the grid-connected inverter output power $\Delta P$ = 1500 W. Fig. 11 presents the simulation waveforms of the inverter terminal voltage when the grid inductance is changed. The grid inductance detection values and accuracy are shown in Table III.

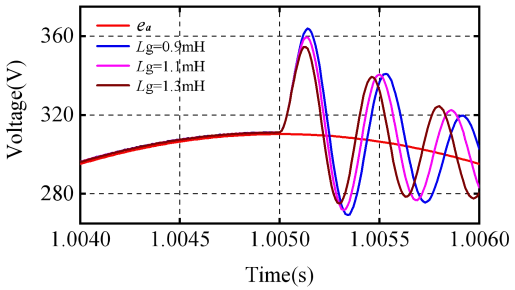


Fig. 11. Simulation waveforms of the inverter terminal voltage ($u_a$) and grid voltage ($e_a$) when grid inductance changes.

TABLE III
SIMULATION RESULTS OF DIFFERENT LINE INDUCTANCE

| Actual Value (mH) | Detection Value (mH) | Accuracy (%) |
|---|---|---|
| 0.9 | 0.842 | 93.5 |
| 1.1 | 1.036 | 94.2 |
| 1.3 | 1.217 | 93.6 |

Based on the simulation results in Fig. 11, the oscillation amplitude and frequency of the inverter terminal voltage both change when grid inductance changes, Detection results in Table III show that grid inductance detection accuracy maintains within the range of 90% - 95%.

To investigate if the sampling and PWM modulation delays (0.075 ms) will affect the oscillation amplitude and frequency of the inverter terminal voltage we have conducted simulations considering the delays. Fig. 12 shows the simulation waveform of the inverter terminal voltage considering and without considering the delays. It can be concluded that the delays slightly affect the voltage amplitude, but do not affect the oscillation frequency of the inverter.

The simulation results show the effectiveness of the proposed theory of grid inductance detection based on the oscillation characteristic of the inverter terminal voltage.

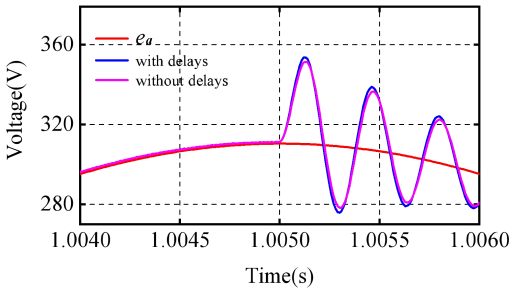


Fig. 12. Simulation waveforms of the inverter terminal voltage ($u_a$) and grid voltage ($e_a$) considering and without considering the delays.

## IV. Experiment Validation

Experiments have been conducted to further validate the effectiveness of the proposed method. Fig. 13(a) illustrates the circuit diagram, and Fig. 13(b) shows the photo of the 10 kW experimental setup of a practical grid-connected PV system. The setup is described in Table IV.

TABLE IV
SETUP OF THE PV EXPERIMENTAL SYSTEM

| Parameters | Symbols | Values |
|---|---|---|
| Filter capacitance | $C_1$ | 3.3 μF |
| Filter inductance | $L_1$ | 2.1 mH |
| Grid inductance | $L_g$ | 2.2 mH |
| Grid resistance | $R_g$ | 63 mΩ |
| Voltage angular frequency | $\omega_1$ | 314 rad/s |
| Grid voltage | $e_x$ | 220 V |
| Proportion coefficient | $K_p$ | 30 |
| Integral coefficient | $K_i$ | 0.1 |
| DC bus voltage | $U_{dc}$ | 680 V |
| PWM frequency | $f_{PWM}$ | 16 kHz |

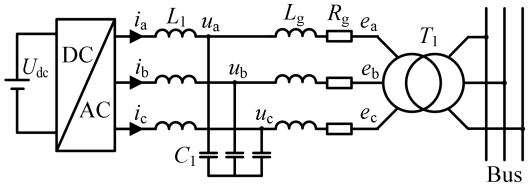


(a)

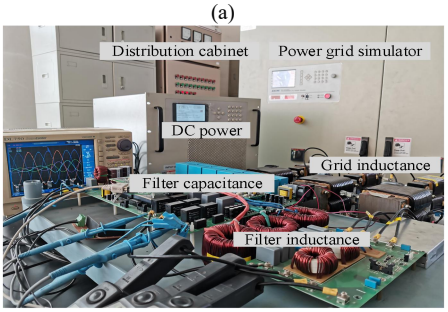


(b)

Fig. 13. Experimental setup. (a) Circuit diagram; (b) Photo.

At the instant of phase $A$'s peak voltage, the grid-connected inverter reference generation power $P_{ref}$ was changed from 1000 W to 2500 W ($\Delta P$ = 1500 W, 15% of the rated capacity). Fig. 14 presents the experimental waveforms of the inverter terminal voltage and grid voltage.

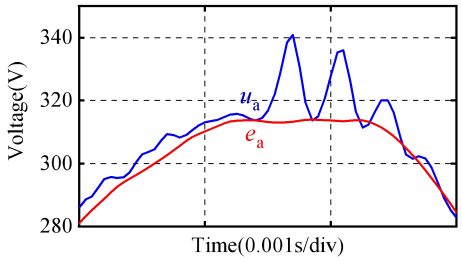


(a)

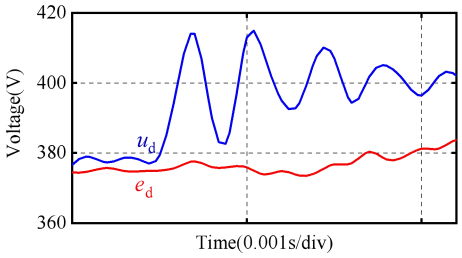


(b)

Fig. 14. Experimental waveforms of the inverter voltages and grid voltage when the inverter output power changed. (a) Inverter terminal voltage ($u_a$) and grid voltage ($e_a$); (b) Inverter terminal voltage ($u_d$) and grid voltage ($e_d$).

Fig. 14 illustrates that when the grid-connected inverter reference generation power $P_{ref}$ steps, $i_d$ rises instantaneously, causing the inverter terminal voltage to oscillate. Substituting the relevant parameters of the experimental system in Table IV into (13), the expression of $u_d$ can be obtained as follow:

$$u_d(t) = 380 - 34.727e^{-14.31t}\cos(11736.31t) + 18.95e^{-14.31t}\sin(11736.31t) - 4.255*10^{-6}e^{-0.08t} + 34.72e^{-4652t} \quad (21)$$

Fig. 14(a) shows the measured inverter terminal voltage oscillation frequency is 2000.47 Hz. From (17), the theoretical calculation oscillation frequency of the inverter terminal voltage is 1868.84 Hz, which shows a relative error of 7.04% compared with the experimental results. The calculation result of the grid inductance $L_g$ is 1.92 mH. Based on the results, the accuracy of the proposed method is 87.3%.

The sudden changes of the grid-connected inverter output power and the grid inductance are conducted to further validate the effectiveness of the proposed method of grid inductance detection. In the experiment, grid inductance $L_g$ is 2.2 mH. Fig. 15 presents the experimental waveforms of the inverter terminal voltage and grid voltage under different sudden changes of the grid-connected inverter output power. The value and accuracy of the grid inductance detection are shown in Table V.

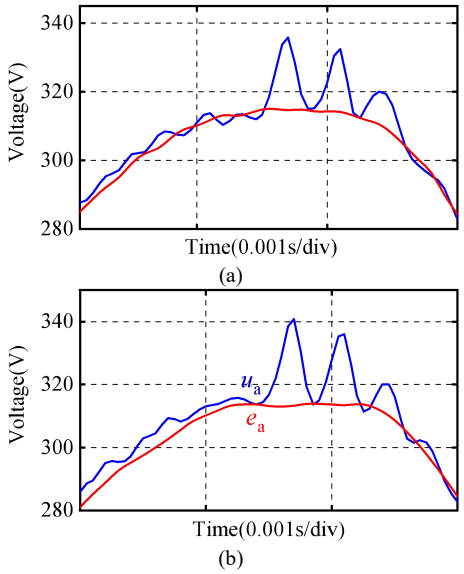


Fig. 15. Experimental waveforms of the inverter terminal voltage ($u_a$) and grid voltage ($e_a$) under different sudden changes of the grid-connected inverter output power changes. (a) $\Delta P$=1000W; (b) $\Delta P$=1500W.

TABLE V
EXPERIMENTAL RESULTS OF DIFFERENT POWER VARIATIONS

| Power Variation (W) | Inductance (mH) | Accuracy (%) |
|---|---|---|
| 1000 | 1.90 | 86.4 |
| 1500 | 1.92 | 87.3 |

In the experiment, the sudden change of the grid-connected inverter output power $\Delta P$ = 1500 W. Fig. 16 presents the experimental waveforms of the inverter terminal voltage and grid voltage when the grid inductance is changed. The grid inductance detection value and accuracy are shown in Table VI.

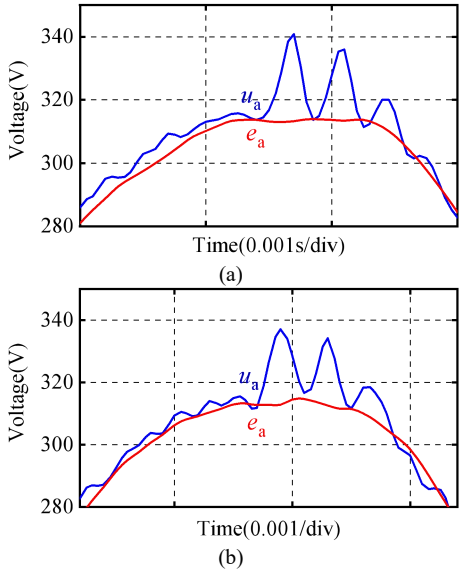


Fig. 16. Experimental waveforms of the inverter terminal voltage ($u_a$) and grid voltage ($e_a$) when grid inductance changes. (a) $L_g$=2.2mH; (b) $L_g$=3.5mH.

Detection results in Table V and Table VI show that the grid inductance detection accuracy maintains within the range of 85%-87%. The experimental results validate the effectiveness of the method of the grid inductance online detection based on the oscillation characteristic of inverter terminal voltage.

TABLE VI
EXPERIMENTAL RESULTS OF DIFFERENT LINE INDUCTANCE

| Actual Value (mH) | Detection Value (mH) | Accuracy (%) |
|---|---|---|
| 2.2 | 1.92 | 87.3 |
| 3.5 | 3.00 | 85.7 |

## V. Conclusion

In this paper, an *LC*-type grid-connected PV system was investigated. An equivalent circuit model of a grid-connected PV system including a controller was established. The oscillation characteristic of the inverter terminal voltage caused by the sudden change of the inverter output power was analyzed. An online detection method of grid inductance based on the oscillation characteristic of the inverter terminal voltage was proposed. The contribution of this method is that it does not need complicated signal processing and calculation procedures. Instead, it only uses the measurement of the oscillation frequency of the inverter terminal voltage. Simulation and experimental results validated the correctness and effectiveness of the proposed method. It will provide a new theoretical basis for grid inductance detection.

## References

[1] T. Strasser, F Andren, and J. Kathan, "A review of architectures and concepts for intelligence in future electric energy systems," *IEEE Trans. Ind. Electron.*, vol. 62, no. 4, pp. 2424-2438, Apr. 2015.

[2] S. Kumar Tiwari, B. Singh, and P. K. Goel, "Design and control of microgrid fed by renewable energy generating sources," *IEEE Trans. Ind. Appl.*, vol. 54, no. 3, pp. 2041-2050, May. 2018.

[3] X. Liang, "Emerging power quality challenges due to integration of renewable energy sources," *IEEE Trans. Ind. Appl.*, vol. 53, no. 2, pp. 855-866, Mar. 2017.

[4] M. Ben Saïd-Romdhane, M. W. Naouar, I. Slama-Belkhodja, and E. Monmasson, "Robust active damping methods for *LCL* filter-based grid-connected converters," *IEEE Trans. Power Electron.*, vol. 32, no. 9, pp. 6739-6750, Sep. 2017.

[5] M. Sumner, A. Abusorrah, D. Thomas, and P. Zanchetta, "Real time parameter estimation for power quality control and intelligent protection of grid-connected power electronic converters," *IEEE Trans. Smart Grid.*, vol. 5, no. 4, pp. 1602-1607, Jul. 2014.

[6] J. Fang, P. Lin, H. Li, and Y. Tang, "A improved virtual inertia control for three-phase voltage source converters connected to a weak grid," *IEEE Trans. Power Electron.*, vol. 34, no. 9, pp. 8660-8670, Sep. 2019.

[7] J. De Kooning, J. Van de Vyver, J. D. M. De Kooning, T. L.Vandoorn, and L.Vandevelde, "Grid voltage control with distributed generation using online grid impedance," *Sustain. Energy, Grids Netw.*, vol. 5, pp.70-77, 2016.

[8] A. Vijayakumanri, A. T. Devarajan, and N. Devarajan, "Decouped control of grid connected inverter with dynamic online grid impedance measurements for micro grid applications," *Int. J. Electr. Power Energy Syst.*, vol. 68, pp. 1-14, 2015.

[9] A. Ghanem, M. Rashed, M. Sumner, M. A. Elsayes, and I. I. I. Mansy, "Grid impedance estimation for islanding detection and adaptive control of converters," *IET Power Electron.*, vol. 10, no. 11, pp 1279-1288, Sep. 2017.

[10] M. Cespedes and J. Sun, "Adaptive control of grid-connected inverters based on online grid impedance measurements," *IEEE Trans. Sustain Energy*., vol. 5, no. 2, pp. 516-523, Apr. 2014.
[11] N. Mohammed, T. Kerekes, and M. Ciobotaru, "An online event-based grid impedance estimation technique using grid-connected inverters," *IEEE Trans. Power Electron.*, vol. 36, no. 5, pp. 6106-6117, May. 2021.
[12] L. Asiminoaei, R. Teodorescu, F. Blaabjerg, and U. Borup, "Implementation and test of an online embedded grid impedance estimation technique for PV inverters," *IEEE Trans. Ind. Electron*., vol. 52, no. 4, pp. 1136-1144, Aug. 2005.
[13] A, V. Timbus, R. Teodorescu, F. Blaabjery, and U. Borup, "Online grid measurement and ENS detection for PV inverter running on highly inductive grid," *IEEE Power Electron. Lett*., vol. 2, no. 3, pp. 77-82, Sep. 2004.
[14] M. Ciobotaru, R. Teodorescu, and F. Blaabjerg, "Online grid impedance estimation based on harmonic injection for grid-connected PV inverter," in *Proc. IEEE Int.Symp. Ind. Electron*., 2007, pp. 2437-2442.
[15] P. García, M. Sumner, Á. Navarro-Rodríguez, J. M. Guerrero and J. García, "Observer-based pulsed signal injection for grid impedance estimation in three-phase systems," *IEEE Trans. Ind. Electron*., vol. 65, no. 10, pp. 7888-7899, Oct. 2018.
[16] T. Roinila, T. Messo, T. Suntio, and M. vilkko, "Pseudo-random sequences in *DQ*-domain analysis of feedforward control in grid-connected inverters," *IFAC-PapersOnLine*, vol. 48, no. 28, pp. 1301-1306, 2015.
[17] A. Riccobono, E. Liegmann, A. Monti, F. Castelli Dezza, J.Siegers, and E Santi, "Online wideband identication of three-phase AC power grid impedances using an existing grid-tied power electronic inverter," *IEEE 17th Work. Control Model. Power Electron*., 2016, pp. 1-8.
[18] S. Neshvad, S. Chatzinotas, and J. Sachau, "Wideband identification of power network parameters using pseudo-random binary sequences on power inverters," *IEEE Trans. Smart Grid.*, vol. 6, no. 5, pp. 2293-2301, Sep. 2015.
[19] A. V. Timbus, R. Teodorescu, and P. Rodriguez, "Grid impedance identification based on active power variation and grid voltage control," in *Proc. IEEE Ind. Appl. Annu. Mee*t., 2007, pp. 949-954.
[20] L. Wang, J. Chen, X. Li, X Sun, and J. M. Guerrero, "Fundamental impedance identification method for grid-connected voltage source inverters," *IET Power Electron*., vol. 7, no. 5, pp. 1099-1105, 2014.
[21] J. H Cho, K. Y.Choi, Y. W. Kim, and R. Y. Kim, "A novel P-Q variations method using a decoupled injection of reference currents for a precise estimation of grid impedance," in *Proc. IEEE Energy Connvers. Congr. Expo*., Nov. 2014, pp. 5059-5064.
[22] N. Mohammed, M. Ciobotaru, and G. Town, "An improved grid impedance estimation technique under unbalanced voltage conditions," in *Proc. IEEE PES Innov. Smart Grid Technol. Eur*., 2019, pp .1-5.
[23] J. Fang, H. Deng and S. M. Goetz, "Grid impedance estimation through grid-forming power converters," *IEEE Trans. Power Electron*, vol. 36, no. 2, pp. 2094-2104, Feb. 2021.
[24] M. A. Azzouz and E. F. El-Saadany, "Multivariable grid admittance identification for impedance stabilization of active distribution networks," *IEEE Trans. Smart Grid.*, vol. 8, no. 3, pp. 1116-1128, May. 2017.
[25] D. K. Alves, R. L. d. A. Ribeiro, F. B. Costa, T. d. O. A. Rocha and J. M. Guerrero, "Wavelet-based monitor for grid impedance estimation of three-phase networks," *IEEE Trans. Ind Electron*, vol. 68, no. 3, pp. 2564-2574, Mar 2021.
[26] S. Cobreces, E. J. Bueno, D. Pizarro, F. J. Rodriguez and F. Huerta, "Grid impedance monitoring system for distributed power generation electronic interfaces," *IEEE Trans. Instrum Meas.*, vol. 58, no. 9, pp. 3112-3121, Sep. 2009.
[27] M. Liserre, F. Blaabjerg and R. Teodorescu, "Grid impedance estimation via excitation of *LCL*-filter resonance," *IEEE Trans. Ind. Appl*., vol. 43, no. 5, pp. 1401-1407, Sep. 2007.
[28] N. Hoffmann and F. W. Fuchs, "Minimal invasive equivalent grid impedance estimation in inductive-resistive power networks using extended kalman filter," *IEEE Trans. Power Electron*., vol. 29, no. 2, pp. 631-641, Feb. 2014.
[29] G. Welch and G. Bishop, "An Introduction to the Kalman Filter," Univ. North Carolina, Chapel Hill, NC, USA, Tech. Rep. TR 95-041, 2004.
[30] V. Valdivia, A. Lázaro, A. Barrado, P. Zumel, C. Fernández and M. Sanz, "Impedance identification procedure of three-phase balanced voltage source inverters based on transient response measurements," *IEEE Trans. Power Electron*., vol. 26, no. 12, pp. 3810-3816, Dec. 2011
[31] A. Vidal et al., "A method for identification of the equivalent inductance and resistance in the plant model of current-controlled grid-tied converters," *IEEE Trans. Power Electron*., vol. 30, no. 12, pp. 7245-7261, Dec. 2015.
[32] Sang-Joon Lee, Jun-Koo Kang and Seung-Ki Sul, "A new phase detecting method for power conversion systems considering distorted conditions in power system," in *Proc. Ind. Appl Conf*., 34 *IAS Annu*, *Meeting*, vol.4, pp. 2167-2172, 1999.

**Shuangming Duan** (Member, IEEE) received the B.Eng. in electronical information science and technology from Northeast Electric Power University, Jilin, China, in 2007, the M.Sc. and Ph.D. in electrical engineering from Northeast Electric Power University, Jilin, China, in 2013 and 2018, respectively.

He is currently an Experimenter in the Department of Electrical Engineering of Northeast Electric Power University. His research interests include control of distributed generation in more-electronics power systems and application of large-scale energy storage technology.

**Bo Xia** received the B.Eng. degree in electrical engineering from Northeast Electric Power University, Jilin, China, in 2019, where he is currently working toward the M.Sc. degree.

His research interest includes control of photovoltaic grid-connected inverter.

**Gangui Yan** (Member, IEEE) received the B.Eng. and M.Sc. degrees in electrical engineering from Northeast Electric Power University, Jilin, China, in 1994 and 1997, respectively, and the Ph.D.. degree in electrical engineering from Tsinghua University, Beijing, China, in 2003.

He is currently a Professor in the Department of Electrical Engineering of Northeast Electric Power University. His research interests include large scale integration of wind power into power systems, photovoltaic generation control and VSC-Based HVDC control.

Dr. Yan is a Vice Chairman of IEEE PES Renewable Systems Integration Satellite Committee-China. He is a senior member of CSEE. He is a secretary of Electrical Engineering Mathematic Council of CSEE. He is selected into the National Hundreds and Thousands of Talents Project. He is a Young and Middle-Aged expert with outstangding contributions from the state. He is a expert enjoying the Special Government Allowance. He is selected as a special professor of "Changjiang Scholars" of the Ministry of Education. He has been awarded two Prizes of "Science and Technology Progress" of Nation.

**Nan Li** received the B.Eng. and M.Sc. degrees in electrical engineering from Northeast Electric Power University, Jilin, China, in 2016 and 2019, respectively.

She is currently an engineer of state grid liaoning extra high voltage company, Shenyang, China. Her research interest includes stability analysis of photovoltaic grid-connected inverter.

**Gen Li** (Member, IEEE) received the B.Eng. degree in Electrical Engineering from Northeast Electric Power University, Jilin, China, in 2011, the M.Sc. degree in Power Engineering from Nanyang Technological University, Singapore, in 2013 and the Ph.D. degree in Electrical Engineering from Cardiff University, Cardiff, U.K., in 2018.

From 2013 to 2016, he was a Marie Curie Early Stage Research Fellow funded by the European Commission's

MEDOW project. He has been a Visiting Researcher at China Electric Power Research Institute and Global Energy Interconnection Research Institute, Beijing, China, at Elia, Brussels, Belgium and at Toshiba International (Europe), London, U.K. He has been a Research Associate at the School of Engineering, Cardiff University since 2017. His research interests include control and protection of HVDC and MVDC technologies, power electronics, reliability modelling and evaluation of power electronics systems.

Dr. Li is a Chartered Engineer in the U.K. He is an Associate Editor of the CSEE Journal of Power and Energy Systems. He is an Editorial Board Member of CIGRE ELECTRA. He is an IET Professional Registration Advisor. His Ph.D. thesis received the First CIGRE Thesis Award in 2018. He is the Vice-Chair of IEEE PES Young Professionals and the Technical Panel Sectary of CIGRE UK B5 Protection and Automation.

**Yi Ding** received the B.Eng. degree in transmission engineering from Northeast Electric Power University, Jilin, China, in 2017, where he is currently working toward the M.Sc. degree.

His research interest includes operation control of Microgrid.